Applied Catalysis B: Environmental 95 (2010) 365–373

Contents lists available at ScienceDirect

Applied Catalysis B: Environmental

journal homepage: www.elsevier.com/locate/apcatb

Highly valuable chemicals production from catalytic upgrading of radiata pine sawdust-derived pyrolytic vapors over mesoporous MFI zeolites

Hyun Ju Park [a], Hyeon Su Heo [a], Jong-Ki Jeon [b], Jeongnam Kim [c], Ryong Ryoo [c], Kwang-Eun Jeong [d], Young-Kwon Park [a,*]

[a] School of Environmental Engineering, University of Seoul, 90 Jeonnong-Dong, Dongdaemun-Gu, Seoul 130-743, Republic of Korea
[b] Department of Chemical Engineering, Kongju National University, 275 Buedae-Dong, Cheonan, Chungnam 330-717, Republic of Korea
[c] Center for Functional Nanomaterials and Department of Chemistry, Korea Advanced Institute of Science and Technology, Daejeon 305-701, Republic of Korea
[d] Green Chemistry Research Division, KRICT, Daejeon 305-600, Republic of Korea

ARTICLE INFO

Article history:
Received 1 February 2009
Received in revised form 23 December 2009
Accepted 19 January 2010
Available online 25 January 2010

Keywords:
Mesoporous MFI zeolite
Gallium
Catalytic upgrading
Fast pyrolysis
BTX aromatics

ABSTRACT

The catalytic upgrading of pyrolytic vapors derived from radiata pine sawdust was carried out over mesoporous MFI zeolite synthesized using an amphiphilic organosilane. Its catalytic activity was compared with those of conventional HZSM-5 and mesoporous material from HZSM-5 (MMZ_{ZSM-5}). The effect of gallium incorporation into mesoporous MFI zeolite on the product distribution and chemical composition of bio-oil was also investigated. The catalysts synthesized were characterized using ICP, XRD, N_2-sorption, NH_3-TPD, and H_2-TPR methods. After catalytic upgrading, products were analyzed by GC–TCD, GC–FID, GC–MS, and Karl Fischer titration. The mesoporous MFI zeolite exhibited the best activity in deoxygenation and aromatization during the upgrading of pyrolytic vapors. In particular, mesoporous MFI zeolite showed high selectivity for highly valuable aromatics, such as benzene, toluene, and xylenes (BTX), even though it decreased the overall organic fraction of the bio-oil. The incorporation of gallium into the mesoporous MFI zeolite increased both the organic fraction of the bio-oil and resistance to coke deposition. Moreover, the selectivity for BTX aromatics was enhanced when the appropriate amount of gallium was introduced.

1. Introduction

The importance of alternative energy development has increased rapidly due to the high international crude oil prices and environmental concerns over global warming being aggravated by the use of fossil fuels. Bio-oil is recognized as one of the representative renewable energy sources because the existing infrastructure in the petroleum industry is available for the production of chemicals or the next-generation hydrocarbon biofuels from bio-oil without significant modification [1]. Moreover, since bio-oil is CO_2 neutral and has a negligible sulfur, nitrogen and ash content, it has fewer adverse effects on the environment during energy production and consumption than conventional fossil fuels. For this reason, considerable efforts have been made to maximize the production of useful bio-oil [2–7]. However, bio-oil is produced as an unstable complex, requiring improvements in quality. Currently, the improvement methods for yielding high quality bio-oil can be classified into two routes: simple physical upgrading (hot-gas filtration, emulsification, and solvent addition), and upgrading with catalysts (hydrotreating, mild hydrotreating, and catalytic vapor cracking) [8]. The latter has been the focus studies thus far because it offers significant improvements ranging from simple stabilization to high quality fuel products [9].

Over the past few decades, a number of studies have examined the upgrading of bio-oil over solid acid catalysts, such as pure and modified zeolites [10–22]. According to these reports, among the various zeolite-based catalysts used, HZSM-5 is the most effective for cracking or reforming bio-oil. The catalytic performance of HZSM-5 has been attributed to the shape-selectivity, ion exchange capacity, and unique solid acid characteristics. However, HZSM-5 with micropores within a 5.1 Å × 5.6 Å range is limited by the low mass transfer rates, particularly in the case of large molecules.

Since the discovery of the mesoporous M41S family [23], MCM-41-based materials have been examined as potential upgrading catalysts in biomass-derived vapors, with the effects of acidity and metal incorporation being the main focus of the investigation [24–28]. Based on their results, it was reported that Al-substituted MCM-41 materials are promising catalysts for the production of high quality bio-oil. More recently, considerable progress has been made in the catalytic pyrolysis of biomass. Highly hydrothermal and stable mesoporous aluminosilicates, MMZ and MSU-S, were applied to the catalytic pyrolysis of biomass [29–31], showing high

* Corresponding author. Tel.: +82 2 2210 5623; fax: +82 2 2244 2245.
E-mail address: catalica@uos.ac.kr (Y.-K. Park).

0926-3373/$ – see front matter © 2010 Elsevier B.V. All rights reserved.
doi:10.1016/j.apcatb.2010.01.015

selectivity for specific compounds as well as excellent catalytic activity. In particular, MMZ materials exhibited remarkable catalytic stability and activity, even after two regenerations. Despite the merit of mesoporosity, MCM-41-type mesoporous materials have lower acidity than microporous aluminosilicate zeolites. The low acidity is due to the amorphous nature of the MCM-41 frameworks, which can only provide weak Brönsted acid sites. However, in bio-oil upgrading, strong Brönsted acid sites play a leading role as the active sites for catalytic cracking and reforming reactions.

Recently, Ryoo and co-workers developed a method for synthesizing highly mesoporous zeolites using organosilane surfactants as the mesopore generating agent [32,33]. Various zeolites, such as MFI, BEA and LTA, were synthesized successfully with a narrow distribution of mesopore diameters. The mesoporous were disordered but the pore diameters were uniform and tunable by the synthesis conditions. In the case of MFI, there was a notable decrease in the concentration of Brönsted acid sites [34]. However, the acidity was sufficient for the presence of mesopores to impart the zeolites with high catalytic activities for the transformation of large molecules exceeding the size of the zeolite micropores [35,36].

The catalytic performance of mesoporous MFI zeolite on the upgrading of Japanese larch bio-oil was evaluated in this preliminary study. However, the much larger mesopores (6.2 nm) of the mesoporous MFI zeolite induced an increase in the concentration of undesirable products, such as polycyclic aromatic hydrocarbons (PAHs) and coke [37]. In order to prevent the formation of undesirable large molecules and increase the amount of BTX compounds, it is important to control the catalyst porosity or modify the catalyst itself.

This study examined the catalytic upgrading of pyrolytic vapors derived from radiata pine sawdust over mesoporous MFI zeolites synthesized using organosilane surfactants with a shorter chain length, which possess high acidity and porosity with catalytic activities comparable to those of an MMZ and conventional HZSM-5. In addition, the effects of Ga-incorporation into the mesoporous MFI catalyst on the product distribution and composition were examined in detail with the aim of increasing the concentration valuable chemicals, such as BTXs.

2. Experimental

2.1. Catalyst preparation

A mesoporous MFI catalyst with a Si:Al molar ratio of 20 was synthesized using the procedure reported in the literature [32,35]. An amphiphilic organosilane, [(3-trimethoxysilyl)propyl] dodecyldimethylammonium chloride (TPDAC) ($[(CH_3O)_3SiC_3H_6N(CH_3)_2C_nH_{2n+1}]Cl$, $n = 12$), was used as a mesopore-directing agent. [(3-Trimethoxysilyl)propyl] hexadecyldimethylammonium chloride (TPHAC) was used to synthesize a larger mesoporous MFI catalyst. For comparison, a mesoporous material from a zeolite (MMZ) with a similar Si:Al molar ratio was prepared using the procedure reported in previous studies [30,31]. A commercially available zeolite, HZSM-5 (Zeolyst International Company), and cetyltrimethylammonium bromide (CTAB) were used as the framework source and template, respectively. Both catalysts were calcined, ion exchanged four times with a 1.0 M ammonium nitrate solution at 80 °C to convert them into the NH_4^+ form, and finally calcined again at 550 °C to convert them to their H^+ form. Hereinafter, the mesoporous MFI catalyst and MMZ material are referred to as Meso-MFI, and MMZ_{ZSM-5}, respectively. Various Ga/Meso-MFI catalysts were prepared using the appropriate amount of an aqueous gallium nitrate (Aldrich, 99.9 purity) solution using the incipient wetness method. The prepared catalysts were dried overnight at 110 °C, calcined in air at 550 °C for 5 h, reduced in a hydrogen stream at 500 °C for 4 h, and finally calcined in air at 550 °C for 5 h to generate the highly dispersed active Ga^{3+} species [38,39].

2.2. Characterization of catalysts

The catalysts synthesized in this study were characterized as follows: the X-ray diffraction (XRD) patterns were obtained with a Cu K_α X-ray source using a Rigaku D/MAX-III instrument at room temperature to determine the catalyst crystallinity. The acidity was examined using the NH_3-temperature-programmed desorption (TPD) method with a TPD/TPR 2900 analyzer (Micromeritics Instrument Co.). Prior to the measurements, the samples were first treated in a He stream at 500 °C and then cooled to 100 °C. NH_3 adsorption was then carried out at 100 °C. After purging the samples in a He stream for 2 h to completely remove the physically adsorbed NH_3, the catalysts were heated to 700 °C at a heating rate of 10 °C/min. The desorbed NH_3 was detected using a thermal conductivity detector (TCD). The reducibility of the Ga-incorporated mesoporous zeolites was examined using the H_2-temperature-programmed reduction (TPR) method with BELCAT. Before the TPR measurements, the samples were treated in a He stream at 110 °C for 30 min, cooled to room temperature, and then reduced in a mixture gas stream of 20% H_2/Ar at a flow rate of 30 mL/min and a heating rate of 5 °C/min to 800 °C. Hydrogen consumption during reduction was detected using a TCD. The N_2 adsorption/desorption isotherms were obtained at −196 °C using a Micromeritics ASAP 2000 with the Brunauer–Emmett–Teller (BET) surface area calculated from the linear portion of the BET plot. The micropore volume and external surface area were evaluated using the t-plot method, and the pore size distribution obtained using the Brunauer–Joyner–Halenda (BJH) model. Inductively coupled plasma analysis was used to determine the Si:Al molar ratio. After upgrading, the amount of coke deposited on the catalysts was determined by thermogravimetric analysis (TGA [TGA 2050, TA Instruments]) in the presence of air at a heating rate of 5 °C/min.

2.3. Reaction procedure

Radiata pine, which is a representative wood species in Korea, was used in the catalytic upgrading of wood-derived pyrolytic vapors. The sawdust used in these experiments was screened to size ranges of 0.3–0.5, 1.0–1.7, and 1.7–2.4 mm, and dried in an oven (J-NDS1, JISICO) at 110 °C for 24 h to minimize the water in the oil product. After drying, the water content in all wood sawdust was <1 wt.%. Table 1 lists the characteristics of the radiata pine sawdust used in this study.

The pyrolysis of radiata pine sawdust and subsequent catalytic upgrading of pyrolytic vapors were carried out in a fixed bed reactor system. Fig. 1 shows a schematic diagram of the pyrolysis and catalytic upgrading apparatus. The upgrading system was installed consecutively at the latter part of the main pyrolysis reactor. The main pyrolysis reactor was U-type quartz with an inner volume of 50 mL, a height of 160 mm, and an internal diameter of 15 mm, into which the radiata pine sawdust (5.0 g) was charged. The fixed catalyst bed reactor was a tubular quartz type, with a height of 70 mm, an internal diameter of 15 mm, and filled with the catalyst (0.5 g). All the catalysts were pelletized, crushed, and screened through standard sieves (1.7–2.4 mm). For non-catalytic pyrolysis, the catalyst was replaced with quartz beads to maintain the same space velocity within the fixed catalyst bed. Prior to the experiments, all experimental systems were purged with inert nitrogen at a flow rate of 50 mL/min for 1 h. Both reactors were indirectly heated electrically to the desired reaction

Table 1
Physicochemical characteristics of radiata pine.

Analysis items	Values
Chemical composition (wt.%)	
Cellulose	44.8
Hemicellulose	34.1
Lignin	27.5
Proximate analysis (wt.%)	
Water	7.6
Combustibles	92.2
Ash	0.2
Ultimate analysis (wt.%)	
C	44.8
H	5.9
N	0.1
O	46.2
S	–

temperature. After both reaction temperatures reached 500 °C, the main pyrolysis reactor was inserted into the furnace. Subsequently, the upgrading reaction continued for 1 h. The temperatures of the experimental systems were adjusted using a PID temperature controller and monitored with two thermocouples (K type). The errors of their average reaction temperatures were within ±5 °C. The apparent residence time of the vapors in the main pyrolysis reactor was ~5 s. The condensable bio-oil was collected in a glass condenser, and cooled to a temperature of −25 °C using a circulator (RW-2025G, JEIO TECH) with ethyl alcohol as the cooling liquid. The non-condensable gases through the quenching system were sampled using Teflon gasbags at 30 min intervals to analyze their composition.

The water content of the as-produced bio-oil was measured using the ASTM E 203 method. A Karl Fischer titrator (Metrohm 787 KF Titrino) was used, along with HYDRANAL Composite 5 K (Riedel-de Haen) and HYDRANAL Working Medium K (Riedel-de Haen) as the titration reagent and titration solvent, respectively. The accuracy of the analysis was <1%. For the chemical composition, the bio-oils were centrifuged at 3000 rpm for 5 min with the subsequent separation of the organic fractions from the aqueous. Accurate quantitative-analysis using an external standard method is difficult with existing gas chromatography equipment because bio-oil generally contains hundreds of compounds. However, the area % of a GC–MS chromatogram can be considered to be a good approximation because it indicates the concentrations of chemical compounds in the bio-oil [40]. In this study, quantitative and qualitative analyses of the organic fractions were performed using a GC–MS (HP 5973 *inert*) with a HP-5MS (30 m × 0.25 mm × 0.25 μm) capillary column, and ultra high purity He as the carrier gas. The mass spectra obtained by the GC–MS were interpreted based on an automatic library search (Wiley 7n). The pyrolysis gases were analyzed by GC–TCD and GC–FID (ACME 6000, Young Lin Instruments Co., Ltd.) using a Carboxen 1000 (15 ft × 1/8 in.) and HP-plot Al_2O_3/KCl column.

3. Results and discussion

3.1. Characterization of catalysts

Fig. 2 shows the nitrogen adsorption–desorption isotherms of the mesoporous catalysts. All catalysts showed type IV isotherms. $MMZ_{ZSM\text{-}5}$ exhibited an isotherm analogous to that of a typical mesoporous material, MCM-41, whereas the Meso-MFI zeolite showed a slightly different isotherm from the hexagonal material with an increase in adsorption in the range of P/P_0 = 0.7–0.8. This was attributed to capillary condensation in the open mesopores as described previously [32,35], suggesting that the Meso-MFI zeolite has greater textural porosity than $MMZ_{ZSM\text{-}5}$. In addition, there were no changes in the isotherms of the Meso-MFI zeolites after the incorporation of gallium, as shown in Fig. 2. Table 2 lists the textural properties of the catalysts. The BET surface areas and pore volumes of the Meso-MFI zeolite were much higher than those of the conventional HZSM-5 zeolite. This was attributed to the formation of mesopores, as described previously [35]. In addition, the pore size of the Meso-MFI zeolite was larger than that of $MMZ_{ZSM\text{-}5}$, suggesting that this porosity can allow large molecules, such as pyrolytic vapors derived from the lignocellulosics, to diffuse inside the pores. However, for Ga/Meso-MFI zeolites, the BET surface area of the 1 and 5 wt.% Ga-incorporated zeolites was 12 and 20% lower than that of undoped zeolite, respectively (Table 2). It is believed that the majority of gallium species were deposited on the external crystal surface of Meso-MFI. STEM analysis will be carried out in future experiments to prove this speculation. The gallium species in the catalyst prepared by impregnation or ion exchange followed calcination are most likely

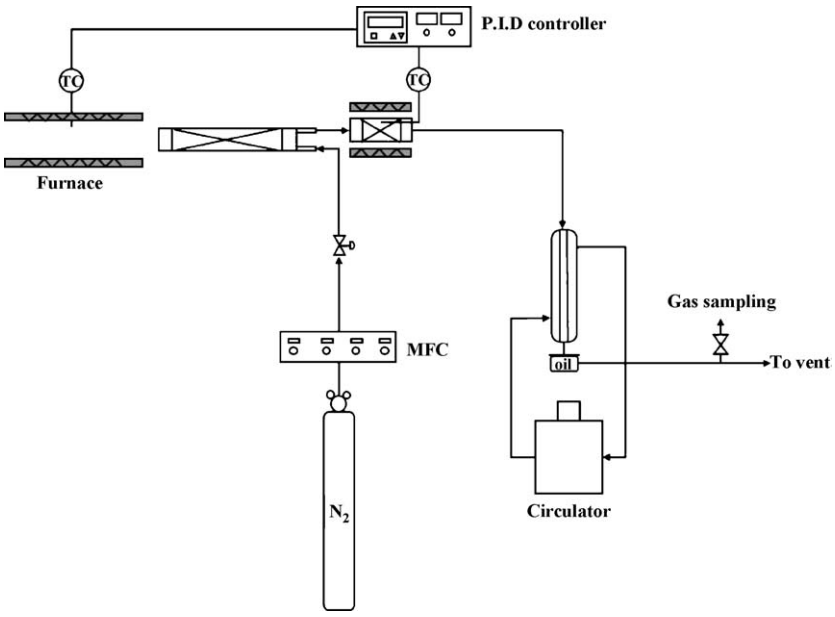

Fig. 1. Schematic diagram of catalytic upgrading apparatus.

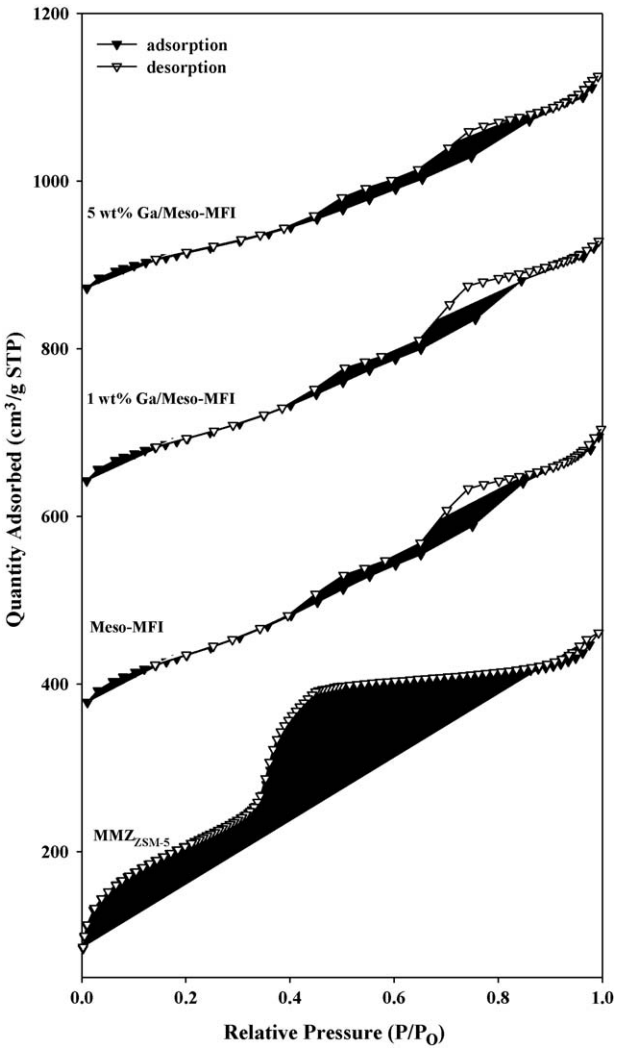

Fig. 2. N_2 adsorption–desorption isotherms of mesoporous catalysts.

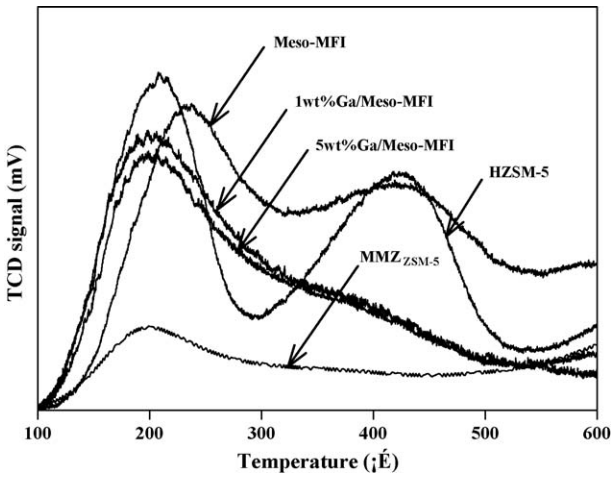

Fig. 3. NH_3-TPD curves of catalysts.

Table 3
NH_3-TPD data at high temperature peak.

Sample	High temperature peak (~400 °C) (mmol g^{-1})
Meso-MFI	0.53
1 wt.% Ga/Meso-MFI	0.28
5 wt.% Ga/Meso-MFI	0.22
HZSM-5	0.35

to be Ga_2O_3 particles that have formed a separate phase or have been deposited at the external crystal surface [41].

Fig. 3 shows the NH_3-TPD curves of the catalysts used in this study. With the exception of MMZ_{ZSM-5}, the other MFI-based catalysts showed two major peaks. The peaks at approximately 230 °C and 420 °C was attributed to NH_3 desorption from the weak acid sites and strong Brönsted acid sites, respectively. The Meso-MFI zeolite showed a distribution of acid sites analogous to that of conventional HZSM-5, whereas the amount and strength of the acid sites in MMZ_{ZSM-5} were much lower than those of the MFI-based zeolites, particularly with the strong acid sites, which might be due to the disordered framework structure and less exposure of Al sites in the MMZ_{ZSM-5} material [30]. After Ga-incorporation on Meso-MFI zeolite, the amount of strong acid sites decreased in proportion to the amount of gallium incorporated, and the low temperature desorption peak at 230 °C was shifted to 200 °C. These shifts were caused by the generation of gallium induced acidic sites (Ga^+–Z^-) as a new active site for aromatization [42]. As mentioned previously, most gallium species are located outside of the Meso-MFI zeolites. However, after reduction by a hydrogen activation treatment, they migrated into the zeolite pores, resulting in the exchange with the protons of the Brönsted acid sites. This can explain the decrease in the number of strong acid sites with increasing Ga loading [41]. These are in accordance with the TPD results (Table 3). Table 3 shows a quantitative evaluation of the acidity as the number of acid sites (mmol/g-cat.), and the high temperature peak area of the 5 wt.% Ga/Meso-MFI catalyst was significantly lower than that of the 1 wt.% Ga/Meso-MFI catalyst.

Fig. 4 shows the high-angle XRD patterns of Meso-MFI zeolites, which are in accordance with the conventional MFI zeolite [32,35]. No gallium species were observed on the Ga-incorporated Meso-MFI zeolites, and there was virtually no decrease in crystallinity, even when the Ga loading was increased to 5 wt.%, suggesting that Ga is well dispersed in the Meso-MFI zeolites. In addition to XRD, TPR measurement is an efficient tool for identifying the various

Table 2
Textural properties of catalysts used in experiments.

Sample	Si/Al[a]	S_{BET}[b] (m^2 g^{-1})	S_t[c] (m^2 g^{-1})	V_P[d] (cm^3 g^{-1})	V_t[e] (cm^3 g^{-1})	d[f] (nm)
HZSM-5	20.1	450	295	0.28	0.14	–
MMZ_{ZSM-5}	18.2	850	–	0.72	–	2.7
Meso-MFI	17.5	647	183	0.67	0.08	4.8
1 wt.% Ga/Meso-MFI	17.5	570	170	0.6	0.08	4.8
5 wt.% Ga/Meso-MFI	17.5	504	172	0.52	0.08	5.1

[a] Measured by ICP-AES analysis.
[b] Calculated in the range of relative pressure (P/P_0) = 0.05–0.20.
[c] Surface area evaluated by the t-plot method.
[d] Measured at P/P_0 = 0.99.
[e] Pore volume evaluated by the t-plot method.
[f] Mesopore diameter calculated by the BJH method.

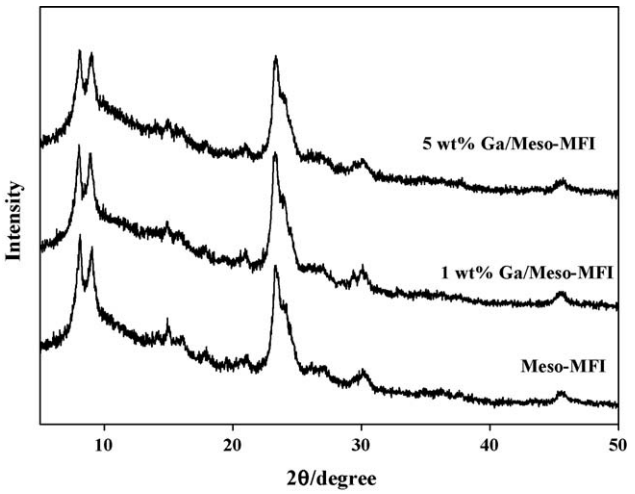

Fig. 4. High-angle XRD patterns of mesoporous MFI zeolites.

states of gallium incorporated into the catalyst. Fig. 5 shows the H_2-TPR profiles of the Meso-MFI zeolites. The reducibility of the Ga-incorporated Meso-MFI zeolites was observed, indicating the presence of non-framework gallium species because framework gallium cannot be reduced at moderate temperatures [39]. Based upon previous report [41], it is also reasonable to expect that these non-framework gallium species would play an important role as actual active sites in the catalytic upgrading of pyrolytic vapors associated with the catalytic performance. The TPR profiles are dominated largely by two major peaks: a peak approximately 420 °C assigned to the reduction of Ga_2O_3 and the other at approximately 620 °C for the reduction of GaO^+ ions. The second peak is pertinent only to the sample with a high Ga loading. Kwak and Sachtler reported similar results and suggested that GaO^+ ions were favored at a high Ga loading [43].

Furthermore, the detailed characterization of the structure and morphology of mesoporous catalysts used in this study has been reported previously [30,32,35]. Briefly, MMZ_{ZSM-5} had a highly ordered hexagonal mesoporous structure similar to that of a classical 2D hexagonal (*P6mm*) mesoporous material, which was identified by low-angle XRD and TEM. In addition, the MAS ^{27}Al

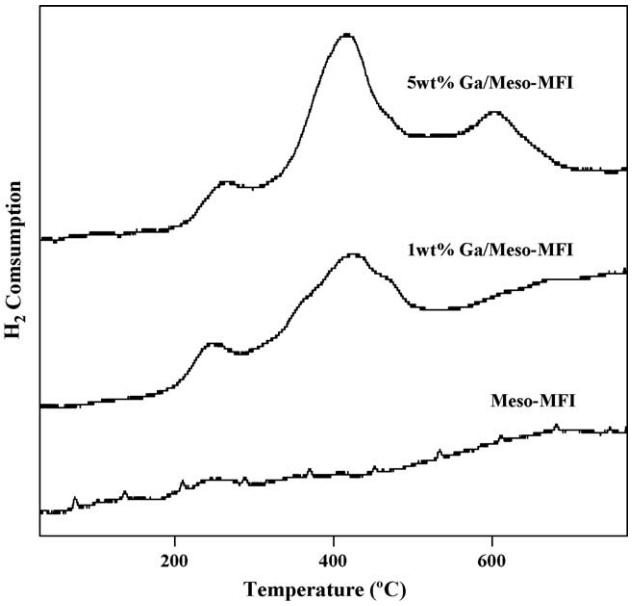

Fig. 5. H_2-TPR profiles of Meso-MFI zeolites.

Table 4
Product distribution from catalytic upgrading of radiata pine sawdust-derived vapors.

Catalyst	Product distribution (wt.%)					Coke[b]
	Bio-oil			Gas	Char	
	Total	Organic fraction	Water content[a]			
Non-catalytic	54.2	16.9	38.8	23.8	22.0	–
HZSM-5	46.6	13.8	52.7	30.4	23.0	13.6
MMZ_{ZSM-5}	50.6	15.1	50.6	27.4	22.0	18.8
Meso-MFI	42.9	11.7	60.8	34.5	22.6	21.3
1 wt.% Ga/Meso-MFI	45.9	13.8	52.4	31.6	22.5	19.4
5 wt.% Ga/Meso-MFI	49.2	15.4	49.5	28.4	22.4	17.3

[a] wt.% on total bio-oil basis.
[b] Obtained by TGA experiments and coke on catalyst.

NMR spectrum suggests that MMZ_{ZSM-5} was synthesized from commercially available HZSM-5 zeolite. The mesoporous structure of the Meso-MFI zeolite is substantiated by the low-angle XRD peak and high resolution SEM and TEM images. The MAS ^{27}Al NMR spectrum of the Meso-MFI zeolite was also in agreement with that of crystalline MFI zeolite.

3.2. Catalytic upgrading of pyrolytic vapors from radiata pine sawdust

Table 4 shows the product distribution after the catalytic upgrading of pyrolytic vapors from radiata pine sawdust. Both the amount of bio-oil and organic fraction yields were significantly lower due to catalytic cracking of the pyrolytic vapors, followed by an increase in gas yields compared to non-catalytic upgrading. Using the catalysts, the water content in the bio-oils also increased drastically and was attributed to bio-oil deoxygenation. Of the catalysts examined, the Meso-MFI zeolite exhibited the highest activity due to the synergic effect of a high porosity and strong acidic property, particularly in the deoxygenation of oxygenated compounds within the bio-oil. However, the high acidity of Meso-MFI zeolite unfortunately induced a decrease in the organic fraction. This drawback could be solved to some extent by the incorporation of gallium into the catalyst. In particular, the 5 wt.% Ga/Meso-MFI zeolite increased the organic fraction to a level similar to that obtained with MMZ_{ZSM-5} due to less cracking of the pyrolytic vapors by the significant decrease in the number of Brönsted acid sites through the incorporation of gallium, as observed in the NH_3-TPD experiments. After catalytic upgrading, the amount of coke deposited on the catalysts depended significantly on the pore size. The microporous HZSM-5 showed the best coke resistance, followed in order by MMZ_{ZSM-5} and Meso-MFI zeolites. The coke yield decreased gradually with increasing gallium content, indicating that the durability against catalyst deactivation was enhanced by the fewer Brönsted acid sites as a result of the replacement of H^+ with gallium species.

The effect of reaction conditions on product distribution was investigated as shown in Tables 5–8. The yields of oil slightly decreased as temperature increased for all the catalysts and that kind of effect was highest for the Meso-MFI catalyst. Also, the yield of oil increased as reaction time increased. But after 20 min, the product distributions were nearly constant for all the catalysts. In addition, the effects of catalyst pellet size and sawdust size on product distribution were negligible.

3.3. Chemical composition of upgraded bio-oils

The bio-oil quality can be evaluated through the chemical composition. Until now, many researchers have classified the different bio-oil organic compounds into desirables, such as phenolics, alcohols and hydrocarbons, and undesirables, such as

Table 5
The effect of catalytic pyrolysis temperature on the product distribution.

Catalyst	Product	Catalyst temperature (°C)		
		300	400	500
		Yield (wt.%)		
HZSM-5	Oil	47.8	47.2	46.6
	Gas	29.0	29.6	30.4
	Char	23.2	23.2	23.0
MMZ_{ZSM-5}	Oil	53.6	51.6	50.6
	Gas	24.4	26.6	27.4
	Char	22.0	21.8	22.0
Meso-MFI	Oil	47.5	47.0	42.9
	Gas	29.9	30.6	34.5
	Char	22.6	22.4	22.6
1 wt.% Ga/Meso-MFI	Oil	48.1	47.1	45.9
	Gas	29.2	30.4	31.6
	Char	22.7	22.5	22.5

Table 6
The effect of reaction time on the product distribution.

Catalyst	Product	Reaction time (min)			
		5	10	20	60
		Yield (wt.%)			
HZSM-5	Oil	42.4	43.6	46.4	46.6
	Gas	31.8	32.0	30.6	30.4
	Char	25.8	24.4	23.0	23.0
MMZ_{ZSM-5}	Oil	45.8	48.2	50.2	50.6
	Gas	28.6	27.8	28.0	27.4
	Char	25.6	24.0	21.8	22.0
Meso-MFI	Oil	39.6	41.1	42.5	42.9
	Gas	35.0	34.9	34.9	34.5
	Char	25.4	24.0	22.6	22.6
1 wt.% Ga/Meso-MFI	Oil	43.1	44.3	45.5	45.9
	Gas	31.4	31.6	31.8	31.6
	Char	25.5	24.1	22.7	22.5

Reaction temperature: 500 °C.

acids, carbonyls, polycyclic aromatic hydrocarbons (PAHs) and heavier oxygenates [27,28,30,31]. In the present study, the bio-oil chemical composition was largely divided into oxygenates, including acids and other oxygen-bonded compounds, mono aromatics, polycyclic aromatic hydrocarbons (PAHs), and phenolics. Generally, these compounds should be removed because

Table 7
The effect of catalyst pellet size on the product distribution.

Catalyst	Product	Catalyst pellet size (mm)		
		0.3–0.5	1.0–1.7	1.7–2.4
		Yield (wt.%)		
HZSM-5	Oil	46.2	45.8	46.6
	Gas	30.7	31.0	30.4
	Char	23.1	23.2	23.0
MMZ_{ZSM-5}	Oil	50.1	50.4	50.6
	Gas	27.7	27.6	27.4
	Char	22.2	22.0	22.0
Meso-MFI	Oil	42.4	42.1	42.9
	Gas	35.3	35.1	34.5
	Char	22.3	22.2	22.6
1 wt.% Ga/Meso-MFI	Oil	45.7	45.5	45.9
	Gas	31.9	31.8	31.6
	Char	22.4	22.7	22.5

Reaction temperature: 500 °C.

Table 8
The effect of sawdust size on the product distribution.

Catalyst	Product	Sawdust size (mm)		
		0.3–0.5	1.0–1.7	1.7–2.4
		Yield (wt.%)		
HZSM-5	Oil	46.0	46.3	46.6
	Gas	31.0	30.8	30.4
	Char	23.1	22.9	23.0
MMZ_{ZSM-5}	Oil	50.5	50.1	50.6
	Gas	27.7	27.7	27.4
	Char	21.8	22.2	22.0
Meso-MFI	Oil	42.4	42.5	42.9
	Gas	35.6	34.7	34.5
	Char	22.0	22.8	22.6
1 wt.% Ga/Meso-MFI	Oil	45.8	46.0	45.9
	Gas	31.9	31.3	31.6
	Char	22.2	22.7	22.5

Reaction temperature: 500 °C.

oxygenates such as carbonyls and acids are responsible for many side-reactions during storage. Of the hydrocarbons, most PAHs are well known toxic and mutagenic compounds, whereas mono aromatics, such as benzene, toluene, ethyl benzene and xylenes, can be considered highly valuable chemicals due to their commercial applicability in the petrochemical industry. Fig. 6 shows the chemical composition of the bio-oils obtained from radiata pine sawdust through non-catalytic pyrolysis and catalytic upgrading. Using the catalysts, the concentration of undesirable oxygenates was reduced significantly compared to non-catalytic pyrolysis, particularly in the case of zeolites with strong acidic properties. In addition, the strong acidic zeolites produced various aromatic hydrocarbons, whereas MMZ_{ZSM-5} containing predominantly weak acid sites did not. In particular, the Meso-MFI zeolites exhibited higher selectivity for the production of aromatics superior to HZSM-5 due to the facile accessibility of large molecules. However, as shown in Table 9, Meso-MFI (C16) with much larger mesopores (6.2 nm) [37] showed higher selectivity for undesirable PAHs than Meso-MFI, indicating that the mesopore size of Meso-MFI zeolite should be controlled appropriately for the selective formation of desirable products over undesirable ones.

Fig. 6 and Table 9 show that the incorporation of gallium into the catalyst affects the aromatics and oxygenates. The selectivity for mono aromatics had no direct dependence on the gallium content. The 1 wt.% Ga/Meso-MFI zeolite increased the mono aromatics yield to 38 wt.%, of which benzene, toluene, and xylenes (BTX) aromatics accounted for 57%. However, 5 wt.% Ga/Meso-MFI decreased it to 18 wt.%. This is likely due to more reduction of protons through incorporation of the excess gallium, leading to a decrease in alkenes acting as precursors of aromatics. Moreover, 5 wt.% Ga/Meso-MFI zeolite increased the oxygenate yield to the level of that obtained with MMZ_{ZSM-5}. Therefore, the catalytic activity for deoxygenation and the selectivity for desirable compounds, such as mono aromatics, are dependent on a combination of strong acid sites and the gallium content. It seems that 1 wt.% Ga/Meso-MFI catalyst maintain the optimum Brönsted acid sites and Ga amount. It is known that maintaining optimum amount of Lewis acid sites induced by Ga and Brönsted acid sites is very important for the aromatization of light alkanes. Kwak reported that Brönsted acid sites catalyze oligomerization and ring closure, but Ga, in concern with protons, acts as a dehydrogenating site. Optimum yields are obtained with catalysts having $Ga/(Ga + H^+)$ ratios between 0.4 and 0.5 [43]. Activity of 5 wt.% Ga/Meso-MFI catalyst decreased due to its lower amount of Brönsted acid sites and reduction of surface area and pore volume by 20% could be another reason of lower activity because the residual

Table 9
Main aromatics identified in bio-oils.

Compound	Distribution (wt.% on organic fraction)						
	Non-catalytic	HZSM-5	MMZ_{ZSM-5}	Meso-MFI	Meso-MFI (C16)[a]	1 wt.% Ga/Meso-MFI	5 wt.% Ga/Meso-MFI
Benzene	–	1.6	0.4	1.7	0.6	2.3	0.4
Toluene	–	4.4	0.5	6.7	4.9	7.8	2.1
Ethyl benzene	–	0.6	–	1.3	0.9	1.6	0.6
m-Xylene	–	5.5	0.6	6.2	6.1	8.5	3.5
p-Xylene	–	1.4	0.2	2.3	2.1	3.3	1.6
C_{9+} mono aromatics	–	6.8	0.3	10.0	10.0	14.8	9.9
C_{10+} PAHs	–	6.5	–	5.0	10.3	4.4	4.8

[a] Synthesized by [(3-trimethoxysilyl)propyl] hexadecyldimethylammonium chloride(TPHAC).

Table 10
Composition of gas products.

Component	Sample					
	Non-catalytic	HZSM-5	MMZ_{ZSM-5}	Meso-MFI	1 wt.% Ga/Meso-MFI	5 wt.% Ga/Meso-MFI
Yield (wt.%)						
CO	8.2	10.7	11.5	13.3	11.3	10.5
CO_2	12.7	15.1	11.9	15.8	14.7	13.7
C_1–C_4	2.9	4.7	3.9	5.5	5.7	4.2
Selectivity (%)						
CH_4	61.8	45.9	56.9	36.9	33.5	42.2
C_2H_4	8.7	14.3	10.7	18.4	20.1	16.3
C_2H_6	11.2	9.7	11.4	7.1	7.3	8.2
C_3H_6	8.5	19.1	11.0	24.3	26.5	20.3
C_3H_8	3.6	4.0	3.7	2.5	2.8	3.0
C_4H_8s	5.2	6.0	5.4	10.0	8.9	9.0
C_4H_{10}s	0.8	0.9	0.8	0.6	0.7	0.9

gallium species sinter and block the aperture and/or the internal channel of zeolite. It should be noted that the polar phenolics are not discussed in this report because only the organic fractions separated were analyzed, even though phenolics can also be another desirable compound.

3.4. Gas products

The incondensable gas products were analyzed quantitatively by GC–TCD and GC–FID (Table 10). The main products were CO, CO_2, and low molecular hydrocarbons within the C_1–C_4 range. The amounts of CO and CO_2 were increased significantly using the catalysts, indicating that the oxygen in bio-oil can be transformed to CO, CO_2 and H_2O. The catalytic activity in the deoxygenation of bio-oil to CO and CO_2 was highest over the Meso-MFI zeolite in a similar manner to deoxygenation by transformation to H_2O. However, compared to the parent zeolites, the Ga-incorporated Meso-MFI zeolites decreased the amount of CO and CO_2 gradually due to the increase in gallium content. This was attributed to a decrease in the number of Brönsted acid sites that play an important role in the cracking of pyrolytic vapors through the introduction of metal. Similar results have been reported elsewhere [44–46]. In addition, after catalytic upgrading, the amount of low molecular hydrocarbons consisting mainly of alkanes and alkenes increased but there was a considerable difference in the distribution of each component according to the catalysts examined. In the case of the strongly acidic zeolites, there was a decrease in the quantity of alkanes, such as methane and ethane, but a drastic increase in the concentration of alkenes, particularly ethene and propene. Moreover, the incorporation of a small amount of Ga into Meso-MFI zeolite resulted in more alkenes. However, the higher gallium content had a slightly negative effect on the formation of alkenes. On the other hand, MMZ_{ZSM-5} with predominantly weak acid sites showed a distribution analogous to a non-catalytic scenario. This can be described with the protolytic mechanism related to the formation of aromatics, as observed previously in the chemical composition of bio-oil.

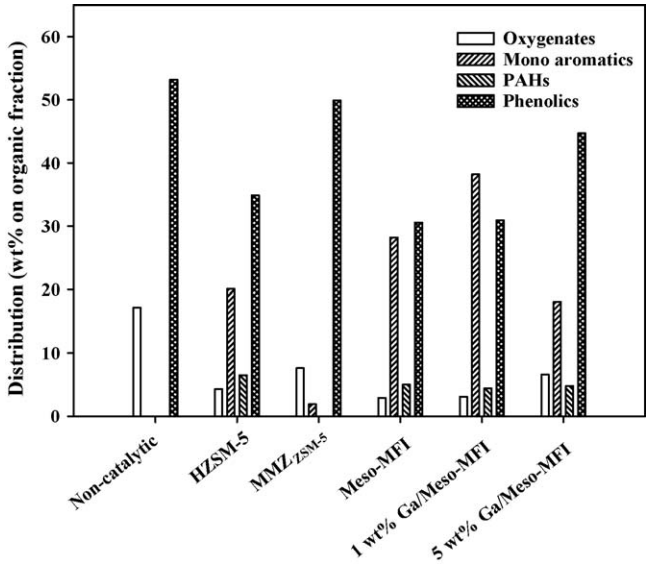

Fig. 6. Chemical composition of bio-oils.

3.5. Aromatization mechanism during catalytic upgrading

Until now, there have been few reports on the formation of aromatics over zeolites, even though a large number of researchers have examined bio-oil upgrading using a variety of zeolites including HZSM-5 [10–12,15,18–20]. However, they did not provide accurate or detailed information on the formation pathway of aromatics. Therefore, another aim of this study was to bring a clearer and well-defined aromatization reaction pathway based on the analysis of gas products. Since the

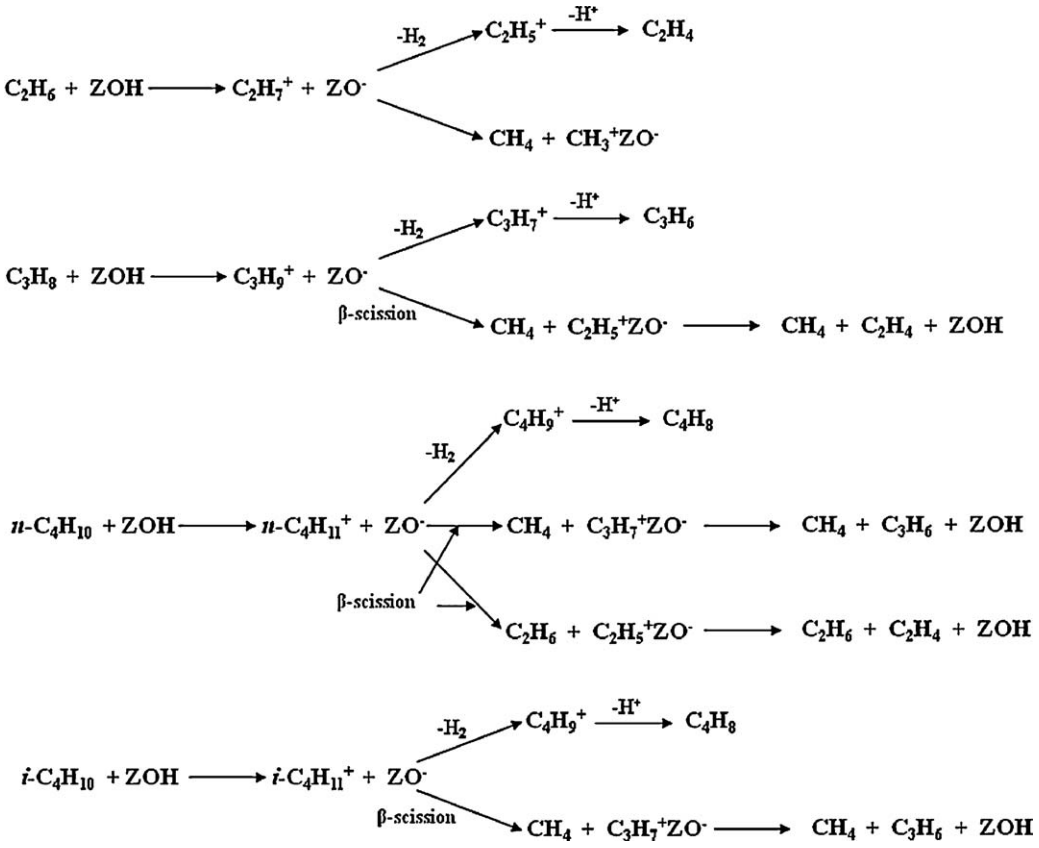

Scheme 1. Activation routes of C_2–C_4 alkanes on HZSM-5.

intermediates formed in the alkane aromatization reaction over HZSM-5 are always C_2–C_4 alkenes, irrespective of the initial carbon number of the feed [47], aromatization during the catalytic upgrading of pyrolytic vapors can be described using an aromatization mechanism of light alkanes, even though in this study different alkanes and alkenes are formed by cracking of the pyrolytic vapors over zeolites. The conversion of light alkanes to highly valuable aromatics has been examined extensively with many studies focusing on the aromatization reaction pathways over medium-pore HZSM-5-based zeolites, including Ga, Zn, and Pt species-incorporated HZSM-5-based zeolites [41,43–58]. According to these examples, the activation of light C_2–C_4 alkanes and subsequent aromatization reaction may proceed through a protolytic mechanism. Firstly, zeolites protonate alkanes at high temperatures to produce unstable carbonium ion transition states that can easily decompose through two different routes: to small alkanes, such as methane, ethane, and propane and carbenium ions *via* protolytic cracking through β-scission; or to H_2 and alkenes, such as ethene, propene and butenes, *via* dehydrogenation. The reaction route is determined by whether the proton attacks a C–C bond or a C–H bond of the alkane. Guisnet et al. analyzed the primary products from the cracking of C_2–C_4 alkanes over H-MFI at 500 °C [59]. Scheme 1 shows a schematic diagram of C_2–C_4 alkane activation on zeolites, such as HZSM-5 and the Meso-MFI, based on their data. The C_2–C_4 alkenes resulting from the protolysis of light alkanes undergo successive oligomerization, cyclization, and dehydrogenation steps, and are finally transformed into aromatic hydrocarbons. From this mechanism, it can be deduced that the amount of aromatics depends on the concentration of alkene precursors in the reaction mixture. Tables 9 and 10 support this deduction. Meso-MFI zeolite showed the highest selectivity for C_2–C_4 alkenes, mainly ethene and propene, and produced the largest amount of aromatics, whereas MMZ_{ZSM-5} with similar selectivity to non-catalytic pyrolysis did not. In addition, the Meso-MFI zeolite showed lower selectivity for C_2–C_4 alkanes than HZSM-5 despite their similar acidity, as observed in the NH_3-TPD experiments, indicating a higher level of alkene production. This is likely due to its higher external surface area, which can increase the level of alkane activation. However, it should be noted that unlike the classical pure alkane aromatization, the large amounts of alkenes in these experiments were formed by the direct decomposition of pyrolytic vapors as well as by the dehydrogenation of alkanes. As a small amount of gallium was incorporated into the Meso-MFI zeolite, the amount of alkenes increased despite the lack of a change in the alkanes, resulting in the production of more aromatics, as shown in Table 9. This suggests that the introduction of Ga species to the Meso-MFI zeolite inhibited the protolytic cracking by β-scission, producing undesirable products, such as methane and leading to dehydrogenation. This is supported by the difference in the amount of methane between 1 wt.% Ga/Meso-MFI and its parent zeolite. It should be noted that the quantity of alkenes increased by only 3% over 1% Ga/Meso-MFI but the amount of aromatics increased to approximately 10%. This was explained by Biscardi and Iglesia [44] who measured the propene hydrogenation/conversion to aromatics rate ratios in propene/propane-2-^{13}C mixtures on metal-incorporated HZSM-5 and concluded that metal cations, such as Ga or Zn increased the propane conversion rates and increased the propene conversion rates even more. Kwak et al. also found that the addition of Ga to HZSM-5 had no effect on the rate of propane cracking, but increased the rate of dehydrogenation [60]. Comprehensive consideration of the above results suggests that the incorporation of Ga cations into Meso-MFI zeolite increases the initial dehydrogenation rates of alkanes as well as subsequent dehydrogenation rates needed to transform the alkenes to aromatics more rapidly, leading to considerably more aromatics compared to that produced by the parent Meso-MFI

zeolite. However, the quantity of alkenes produced decreased with increasing Ga loading due to the reduction of protons acting as active sites for protolysis, resulting in a significant decrease in the concentration of aromatics, as shown in Fig. 6 and Table 9. This was confirmed by Choudhary et al., who investigated the aromatization of dilute ethylene over different Ga-modified HZSM-5 type zeolites and proposed that the zeolites should have both high acidity and an optimum ratio of non-framework Ga to strong acid sites in order for them to be highly active and selective in aromatization [46]. Biscardi and Iglesia also reported the importance of the co-concurrence of Brönsted acid sites in the aromatization of alkanes [44]. Their proposals are in good agreement with these results.

With the use of catalysts, methane selectivity decreased even though pyrolytic cracking occurred, indicating that methane also participates in aromatization. This fact was proved by a few investigations with ^{13}C methane [54,56].

Generally, the aromatization of alkanes or alkenes causes an increase in hydrogen production. However, in this study, the hydrogen yields were <0.3 wt.% even after catalytic upgrading (data not shown). This is important evidence showing that the increase in H_2O in bio-oil after catalytic upgrading is due to the bonding of free oxygen atoms with hydrogen molecules formed during aromatization.

4. Conclusions

Mesoporous MFI zeolite exhibited the best activities, in terms of both deoxygenation and aromatization, during the catalytic upgrading of pyrolytic vapors derived from radiata pine sawdust due to the synergic effect of its high porosity and acidity. In particular, mesoporous MFI zeolite exhibited high selectivity for highly valuable BTX aromatics, even though it decreased both the organic fraction and bio-oil yield. The incorporation of gallium into the mesoporous MFI zeolite resulted in less cracking of the pyrolytic vapors, as well as an increase in the organic fraction of bio-oil and resistance to coke deposition. The amount of gallium incorporated into the mesoporous MFI zeolite played an important role in the selectivity of aromatics. The addition of the appropriate amount of gallium optimized the bifunctional mechanism and the consequent enhancement of the selectivity for BTX aromatics, whereas the excess gallium brought a negative effect on formation of aromatics because of more loss of protons.

Acknowledgment

R.R. acknowledges support from the Korean Ministry of Education, Science and Technology through the National Honor Scientist Program.

References

[1] K. Betts, Environ. Sci. Technol. 42 (2008) 2211.
[2] H.J. Park, J.I. Dong, J.K. Jeon, Y.K. Park, K.S. Yoo, S.S. Kim, J.S. Kim, S.D. Kim, Chem. Eng. J. 143 (2008) 124.
[3] H.J. Park, Y.K. Park, J.I. Dong, J.S. Kim, J.K. Jeon, S.S. Kim, J.S. Kim, B.H. Song, J.H. Park, K.J. Lee, Fuel Process. Technol. 90 (2009) 186.
[4] H.S. Heo, H.J. Park, Y.K. Park, C. Ryu, D.J. Suh, Y.W. Suh, J.H. Yim, S.S. Kim, Bioresour. Technol. 101 (2010) S91.
[5] H.J. Park, H.S. Heo, Y.K. Park, J.H. Yim, J.K. Jeon, J. Park, C. Ryu, S.S. Kim, Bioresour. Technol. 101 (2010) S83.
[6] H.S. Heo, H.J. Park, J.H. Yim, J.M. Sohn, J. Park, S.S. Kim, C. Ryu, Y.K. Park, J.K. Jeon, Bioresour. Technol., doi:10.1016/j.biortech.2009.12.078.
[7] H.S. Heo, H.J. Park, J.I. Dong, S.H. Park, S. Kim, D.J. Suh, Y.W. Suh, S.S. Kim, Y.K. Park, J. Ind. Eng. Chem., doi:10.1016/j.jiec.2010.01.026.
[8] S. Czernik, R. Maggi, G.V.C. Peacocke, in: A.W. Bridgewater (Ed.), Fast Pyrolysis of Biomass: A Handbook, vol. 2, CPL Press, Newbury, 2002, p. 141.
[9] H.J. Park, J.K. Jeon, S.H. Park, J.H. Yim, J.M. Sohn, Y.K. Park, J. Korean Ind. Eng. Chem. 20 (2009) 1.
[10] S. Vitolo, M. Seggiani, P. Frediani, G. Ambrosini, L. Politi, Fuel 78 (1999) 1147.
[11] S. Vitolo, B. Bresci, M. Seggiani, M.G. Gallo, Fuel 80 (2001) 17.
[12] J.D. Adjaye, N.N. Bakhshi, Fuel Process. Technol. 45 (1995) 185.
[13] A.A. Lappas, M.C. Samolada, D.K. Iatridis, S.S. Voutetakis, I.A. Vasalos, Fuel 81 (2002) 2087.
[14] P.T. Williams, P.A. Horne, Fuel 74 (1995) 1839.
[15] P.T. Williams, P.A. Horne, J. Anal. Appl. Pyrol. 31 (1995) 39.
[16] P.T. Williams, P.A. Horne, Fuel 75 (1996) 1051.
[17] P.T. Williams, N. Nugranad, Energy 25 (2000) 493.
[18] R.K. Sharma, N.N. Bakhshi, Bioresour. Technol. 45 (1993) 195.
[19] P.D. Chantal, S. Kaliaguine, J.L. Grandmaison, A. Mahay, Appl. Catal. 18 (1985) 133.
[20] H.J. Park, H.S. Heo, J.H. Yim, J.K. Jeon, Y.S. Ko, S.S. Kim, Y.K. Park, Korean J. Chem. Eng. 27 (2010) 73.
[21] M. Olazar, R. Aguado, J. Bilbao, A. Barona, AIChE J. 46 (2000) 1025.
[22] H.J. Park, J.I. Dong, J.K. Jeon, K.S. Yoo, J.H. Yim, J.M. Sohn, Y.K. Park, J. Ind. Eng. Chem. 13 (2007) 182.
[23] C.T. Kresege, M.E. Leonowicz, W.J. Roth, J.C. Vartuli, J.S. Beck, Nature 359 (1992) 710.
[24] F.A. Twaiq, A.R. Mohamed, S. Bhatia, Micropor. Mesopor. Mater. 64 (2003) 95.
[25] F.A. Twaiq, A.R. Mohamed, S. Bhatia, Fuel Process. Technol. 85 (2004) 1283.
[26] J. Adam, M. Blazsó, E. Mészáros, M. Stöcker, M.H. Nilsen, A. Bouzga, J.E. Hustad, M. Grønli, G. Øye, Fuel 84 (2005) 1494.
[27] J. Adam, E. Antonakou, A. Lappas, M. Stöcker, M.H. Nilsen, A. Bouzga, J.E. Hustad, G. Øye, Micropor. Mesopor. Mater. 96 (2006) 93.
[28] E. Antonakou, A. Lappas, M.H. Nilsen, A. Bouzga, M. Stöcker, Fuel 85 (2006) 2202.
[29] K.S. Triantafyllidis, E.F. Iliopoulou, E.V. Antonakou, A.A. Lappas, H. Wang, T.J. Pinnavaia, Micropor. Mesopor. Mater. 99 (2007) 132.
[30] H.I. Lee, H.J. Park, Y.K. Park, J.Y. Hur, J.K. Jeon, J.M. Kim, Catal. Today 132 (2008) 68.
[31] H.J. Park, J.K. Jeon, J.M. Kim, H.I. Lee, J.H. Yim, J.H. Park, Y.K. Park, J. Nanosci. Nanotechnol. 8 (2008) 5439.
[32] M. Choi, H. Cho, R. Srivastava, C. Venkatesan, D. Choi, R. Ryoo, Nat. Mater. 5 (2006) 718.
[33] M. Choi, R. Srivastava, R. Ryoo, Chem. Commun. (2006) 4380.
[34] K. Suzuki, Y. Aoyagi, N. Katada, M. Choi, R. Ryoo, M. Niwa, Catal. Today 132 (2008) 38.
[35] V.N. Shetti, J. Kim, R. Srivastava, M.K. Choi, R. Ryoo, J. Catal. 254 (2008) 296.
[36] R. Srivastava, M. Choi, R. Ryoo, Chem. Commun. (2006) 4489.
[37] K.H. Park, H.J. Park, J. Kim, R. Ryoo, J.K. Jeon, J. Park, Y.K. Park, J. Nanosci. Nanotechnol. 10 (2010) 355.
[38] K.M. Dooley, C. Chang, G.L. Price, Appl. Catal. A: Gen. 84 (1992) 17.
[39] S.A. Hamid, E.G. Derouane, G. Demortier, J. Riga, M.A. Yarmo, Appl. Catal. A: Gen. 108 (1994) 85.
[40] M.C. Samolada, A. Papafotica, I.A. Vasalos, Energy Fuels 14 (2000) 1161.
[41] R. Fricke, H. Kosslick, G. Lischke, M. Richter, Chem. Rev. 100 (2000) 2303.
[42] C. Chang, M.D. Lee, Appl. Catal. A: Gen. 123 (1995) 7.
[43] B.S. Kwak, W.M.H. Sachtler, J. Catal. 145 (1994) 456.
[44] J.A. Biscardi, E. Iglesia, J. Catal. 182 (1999) 117.
[45] A. Smiešková, E. Rojasová, P. Hudec, L. Šabo, Appl. Catal. A: Gen. 268 (2004) 235.
[46] V.R. Choudhary, P. Devadas, S. Banerjee, A.K. Kinage, Micropor. Mesopor. Mater. 47 (2001) 253.
[47] N. Viswanadham, G. Muralidhar, T.S.R.P. Rao, J. Mol. Catal. A: Chem. 223 (2004) 269.
[48] O.V. Chetina, T.V. Vasina, V.V. Lunin, Appl. Catal. A: Gen. 131 (1995) 7.
[49] S. Todorova, B.L. Su, J. Mol. Catal. A: Chem. 201 (2003) 223.
[50] D. Bhattacharya, S. Sivasanker, Appl. Catal. A: Gen. 141 (1996) 105.
[51] S. Todorova, B.L. Su, Catal. Today 93 (2004) 417.
[52] G.V. Echevsky, E.G. Kodenev, O.V. Kikhtyanin, V.N. Parmon, Appl. Catal. A: Gen. 258 (2004) 159.
[53] M.C.J. Bradford, M. Te, M. Konduru, D.X. Fuentes, Appl. Catal. A: Gen. 266 (2004) 55.
[54] X.C. Shen, H. Lou, K. Hu, X.M. Zheng, Chin. Chem. Lett. 18 (2007) 479.
[55] J. Guo, H. Lou, H. Zhao, L. Zheng, X. Zheng, J. Mol. Catal. A: Chem. 239 (2005) 222.
[56] J.F. Liu, Y. Liu, L.F. Peng, J. Mol. Catal. A: Chem. 280 (2008) 7.
[57] C. Bigey, B.L. Su, J. Mol. Catal. A: Chem. 209 (2004) 179.
[58] F. Lemos, M. Guisnet, F.R. Ribeiro, J. Mol. Catal. A: Chem. 255 (2006) 131.
[59] M. Guisnet, N.S. Gnep, D. Aittaleb, Y.J. Doyemet, Appl. Catal. A: Gen. 87 (1992) 255.
[60] B.S. Kwak, W.M.H. Sachtler, W.O. Haag, J. Catal. 149 (1994) 465.